⌘ *Author's Choice*

THE JOURNAL OF BIOLOGICAL CHEMISTRY VOL. 286, NO. 14, pp. 12650–12658, April 8, 2011

Structure and Interactions of Myosin-binding Protein C Domain C0

CARDIAC-SPECIFIC REGULATION OF MYOSIN AT ITS NECK?[*] [S]

Received for publication, June 23, 2010, and in revised form, January 10, 2011 Published, JBC Papers in Press, February 5, 2011, DOI 10.1074/jbc.M110.156646

Joyce Ratti[‡1], **Elena Rostkova**[§2], **Mathias Gautel**[§2], **and Mark Pfuhl**[‡3]

From the [‡]*Department of Biochemistry, University of Leicester, Lancaster Road, Leicester LE1 9HN and the* [§]*Randall Division for Cell and Molecular Biophysics and Cardiovascular Division, King's College London, British Heart Foundation (BHF) Centre of Research Excellence, London SE1 1UL, United Kingdom*

Myosin-binding protein C (MyBP-C) is a multidomain protein present in the thick filaments of striated muscles and is involved in both sarcomere formation and contraction regulation. The latter function is believed to be located at the N terminus, which is close to the motor domain of myosin. The cardiac isoform of MyBP-C is linked to hypertrophic cardiomyopathy. Here, we use NMR spectroscopy and biophysical and biochemical assays to study the three-dimensional structure and interactions of the cardiac-specific Ig-like domain C0, a part of cardiac MyBP-C of which little is known. The structure confirmed that C0 is a member of the IgI class of proteins, showing many of the characteristic features of this fold. Moreover, we identify a novel interaction between C0 and the regulatory light chain of myosin, thus placing the N terminus of the protein in proximity to the motor domain of myosin. This novel interaction is disrupted by several cardiomyopathy-linked mutations in the MYBPC3 gene. These results provide new insights into how cardiac MyBP-C incorporates in the sarcomere and how it can contribute to the regulation of muscle contraction.

Muscle contraction occurs as the result of many sarcomeric proteins interacting with one another in a precise manner. The main interacting system is formed by myosin and actin, with proteins such as troponin and tropomyosin being essential for regulation. Other proteins have in recent years become established as additional regulatory proteins in muscle contraction, one of them being myosin-binding protein C (MyBP-C)[4] (1–3), a multidomain protein formed of immunoglobulin I (IgI) and fibronectin type III domains, similarly to titin (Fig. 1). Three isoforms exist of MyBP-C, for fast skeletal, slow skeletal, and cardiac muscle (4). The cardiac form presents some unique features such as the long insertion in the CD loop of domain C5 (5, 6), the insertion of two extra phosphorylation sites in the MyBP-C motif, located at the N terminus between domains C1 and C2, and an extra domain at its N terminus (C0) (5). MyBP-C was suggested to function as a tether that holds on to myosin heads close to the S1-S2 neck region through its N terminus (7–10) in a phosphorylation-regulated manner involving the MyBP-C motif (10, 11). The observation that short N-terminal fragments of MyBP-C, too short to perform a tethering role, are also able to influence S1 activity hinted at an additional, more direct way in which MyBP-C could regulate muscle contraction (11–13). Recently, we positioned the binding site for MyBP-C domain C1 right next to the S1-S2 hinge in immediate proximity to the regulatory light chain (14). As domain C2 is located further C-terminal on S2 (15), it would be plausible to look for an interaction site for the most N-terminal domain of MyBP-C further N-terminally on myosin. An interaction between the cardiac isoform of MyBP-C and the regulatory light chain (RLC) of myosin has been proposed as early as 1985 (16). Most likely, such an interaction might take place via the cardiac-specific domain C0. This would be entirely in agreement with results obtained with short, N-terminal MyBP-C fragments because these contained domain C0 (11–13). The assumption would be that these fragments somehow influence myosin activity via the RLC. The RLC is positioned in the neck region of myosin and, together with the essential light chain (ELC), stabilizes the 8.5-nm-long end of the lever helix by wrapping around it (17, 18) in the region spanning residues 808 and 842 (Fig. 1). The RLC seems to be of great importance for both myosin structure and function. Selective removal of the RLC causes a change in the structure of the cardiac myosin molecule (19), leading to myosin disorder (9) and, importantly, weakens binding to MyBP-C (16). The RLC is also phosphorylated at its N terminus upon adrenergic stimulation (20), although the relevance of this in cardiac muscle, in contrast to *e.g.* smooth muscle, is not completely understood (21–23). The regulatory light chain is a member of the superfamily of EF-hand Ca^{2+}-binding protein and is also linked to hypertrophic cardiomyopathy (HCM), with currently seven known mutations that are linked to hereditary cardiac disease (UniProtKB/Swiss-Prot accession

[*] This work was supported by a BHF studentship (to M. P.) and the Medical Research Council of Great Britain (to M. G.).

⌘ *Author's Choice*—Final version full access.

The atomic coordinates and structure factors (code 2K1M) have been deposited in the Protein Data Bank, Research Collaboratory for Structural Bioinformatics, Rutgers University, New Brunswick, NJ (http://www.rcsb.org/).

[S] The on-line version of this article (available at http://www.jbc.org) contains supplemental Figs. S1–S3.

[1] Both authors contributed equally to this work.

[2] Holds the British Heart Foundation Chair of Molecular Cardiology.

[3] To whom correspondence should be addressed:, King's College London, Randall Division for Cell and Molecular Biophysics and Cardiovascular Division, BHF Centre of Research Excellence, London SE1 1UL, UK. Tel.: 44-20-7848-6478; E-mail: Mark.Pfuhl@kcl.ac.uk.

[4] The abbreviations used are: MyBP-C, myosin-binding protein C; MyBS, binding site on myosin for the regulatory light chain; RLC, regulatory light chain; ELC, essential light chain; DSC, differential scanning calorimetry; ITC, isothermal titration calorimetry; HCM, hypertrophic cardiomyopathy; r.m.s.d., root mean square displacement; TOCSY, total correlation spectroscopy; HSQC, heteronuclear single quantum correlation.

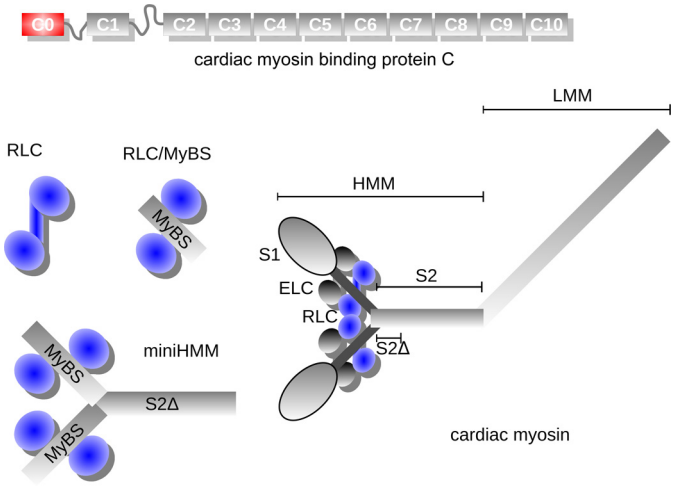

FIGURE 1. **Overview of cardiac myosin and MyBP-C depicted in *gray drawings* on the *right* (domain C0 and the RLC are highlighted in *red* and *blue*, respectively) and the constructs representing them used in this work.** RLC is the regulatory light chain by itself. RLC-MyBS is the RLC bound to its binding site on myosin (residues 806–835). miniHMM is a shortened version of the well established HMM fragment of myosin lacking S1, ELC, and the C-terminal three-quarters of the S2 fragment (residues 806–963 of myosin). One RLC is bound per binding site. *HMM*, heavy meromyosin; *LMM*, light meromyosin.

number P10916). Several different genes exist for RLC encoding numerous isoforms, among others, for cardiac and skeletal muscle, similar to MyBP-C. In the present work, our focus has been determining the structure of the cardiac-specific domain C0 and studying its interaction with the S1 fragment of myosin and more precisely with the regulatory light chain that associates with it. MyBP-C and RLC, together with other sarcomeric proteins, are both linked to HCM, a genetic disorder leading to cardiac dysfunction that can manifest itself through arrhythmias, heart failure, and sudden cardiac death, especially in the young. Domain C0 shows three missense mutations linked to HCM in human (Sarcomere Protein Gene Mutation Database and UniProtKB/Swiss-Prot accession number Q14896) and one in Maine Coon cats (24), making it one of the domains presenting the fewest HCM mutations, surprisingly given its unique cardiac nature.

In this work, we study the structure and dynamics of domain C0 and show that it binds to the RLC. We map the binding site and show the effect upon the interaction by some HCM-related mutations. Our biophysical results are backed up by immunofluorescence studies showing C0 co-localizing by itself in the A-band, consistent with an interaction around the myosin heads.

EXPERIMENTAL PROCEDURES

Sample Preparation—Domain C0 (residues 1–95 of human cardiac MyBP-C) was cloned in vector pET8c and expressed and purified as described previously for domain C5 (6). Isotope-enriched samples were produced by expression in M9 minimal medium supplemented with uniformly ^{13}C-enriched glucose (CIL) and/or [^{15}N]ammonium chloride (CIL) as unique sources of carbon and nitrogen, respectively. The four mutants produced for the mutagenesis studies were cloned in vector pLEICS-03 (available from the Protex laboratory at the University of Leicester) and expressed in LB medium as wild type.

The miniHMM heavy chain construct contains residues 806–963 of the cardiac β-myosin heavy chain (NM_000257). The fragment contains the RLC binding site (residues 806–835) and the N-terminal part of the coiled-coil myosin rod, S2Δ (848–963) (10). The myosin fragment was cloned into a modified pET8c vector with ampicillin resistance containing a His_6 tag and tobacco etch virus protease cleavage site. This fragment was impossible to express on its own, probably due to its instability caused by the very likely unfolded RLC binding site. In contrast, the S2Δ fragment alone was easily expressed in *Escherichia coli* with a high yield as described previously (25). To stabilize the RLC binding site, we co-expressed the miniHMM myosin heavy chain fragment with cardiac RLC (GI_4557774) cloned into the pACYC vector with kanamycin resistance. The two plasmids were co-transformed into BL21 [DE3] RIL-competent cells and grown on plates and media containing both antibiotics. Protein was purified using polyhistidine binding nickel chelate resin (HiTrap) by standard procedures. The purified protein was cleaved by tobacco etch virus protease, and tag, uncleaved protein, and tobacco etch virus protease were removed by one pass over a nickel HiTrap. The same procedure was used for cloning and expression of the RLC binding site cloned in pET8c and co-expressed with the RLC.

NMR Spectroscopy—Different samples were prepared to perform the NMR experiments: [^{13}C/^{15}N C0] = 1.4 mM, [^{15}N C0] = 670 μM, [$C0_{Ar}$] = 1.7 mM in 50 mM phosphate buffer at pH 7 containing 50 mM NaCl, 2 mM DTT, and 0.01% NaN_3. The first, doubly labeled sample was used to record the triple resonance experiments, HNCaCb, HN(CO)CaCb, HN(Ca)CO, HNCO, HN(CaCb)HaHb, HN(CaCbCO)HaHb (26–28), and the ^{13}C-specific experiments such as ^{1}H/^{13}C HSQC, ^{1}H/^{13}C HCCH TOCSY (29), and ^{1}H/^{13}C NOESY-HSQC (30); from the ^{15}N-enriched sample were obtained ^{1}H/^{15}N HSQC, ^{1}H/^{15}N TOCSY-HSQC, and ^{1}H/^{15}N NOESY-HSQC. An unlabeled sample was used to record the spectra relative to the aromatic side chains ^{1}H/^{1}H TOCSY and ^{1}H/^{1}H nuclear Overhauser enhancement spectroscopy (NOESY). The NMR samples were concentrated in Vivaspin 20 concentrators with 3-kDa molecular mass cutoff (Sartorius) and transferred to a clean NMR tube (Shigemi). The ^{13}C/^{15}N C0 and $C0_{Ar}$ samples were frozen and lyophilized overnight to eliminate the water and then resuspended in high purity D_2O (Sigma). All NMR spectra were obtained using in-house modified pulse sequences based on the standard pulse sequences provided by Bruker. They were collected on Bruker Avance spectrometers at 600 MHz, with and without cryoprobe, or 800 MHz with cryoprobe at 303 K. NMR spectra were processed with Topspin and analyzed with CCPNMR Analysis software. Sequence-specific assignments were deposited in the Biological Magnetic Resonance Bank (BMRB) with accession code 5679.

Relaxation analysis was performed by measuring ^{15}N R_1, R_2, and ^{1}H-^{15}N heteronuclear NOE experiments (31) on a ^{15}N-labeled sample. R_1 was measured with delays of 16, 48, 96, 192, 288, 384, 512, 704, 880, 1120, and 1440 ms; R_2 was measured with delays of 5, 10, 15, 20, 31, 41, 61, 82, 102, 133, 154 ms. The heteronuclear NOEs were measured with a proton saturation period of 3 s. Relaxation rates were extracted from the time series by exponential fit using customized macros in the pro-

TABLE 1
Structural statistics for domain C0

Input constraints	
Dihedral angle constraints	180
NOE-derived distances	1142
Hydrogen bond constraints	26
Structure statistics	
Backbone r.m.s.d.	0.4 Å
Heavy atom r.m.s.d.	
Residues in core region of Ramachandran plot	83.70%
Residues in allowed region of Ramachandran plot	100.00%
Average/maximal violation of NOE constraints	0.013/0.2 Å
Average/maximal violation of dihedral constraints	0.223/4°

gram Mathematica (Wolfram Research). Relaxation rates were initially used to obtain the rotational correlation time from R_1/R_2. using the value of τ_c obtained, and a Lipari-Szabo analysis (32–34) was performed for all individual residues.

Interaction studies were carried out by measuring ^{1}H-^{15}N HSQC spectra (35) of 50 μM ^{15}N-labeled C0 without and with binding partner, RLC, RLC-MyBS, or miniHMM at a concentration of 200 μM. The experiment was repeated for G5R, R35W, and K87E mutants of C0 under identical conditions. Spectra were recorded at 800 MHz and a temperature of 298 K using standard NMR buffer. For analysis, ^{1}H and ^{15}N chemical shift perturbations were combined according to $\Delta\delta = |\Delta\delta(^1\mathrm{H})| + 0.15 \times |\Delta\delta(^{15}\mathrm{N})|$ (36) and plotted against the sequence. The weighting used in this study is different from that used in previous work on interactions of domains of MyBP-C (14, 15) so that the chemical shift perturbations appear relatively smaller.

Structure Calculation—The automatic assignment of the peaks picked manually in the three-dimensional ^{1}H/^{13}C NOESY HSQC experiment was carried out using the CANDID protocol (37), as part of the software CYANA 2.1 (38). Out of the total 2460 peaks, 88% were assigned (2170), whereas just 292 (12%) were left unassigned at the end of the procedure; all these unassigned peaks were the product of artifacts in the NMR experiments and were all checked manually at the end of the automatic assignment procedure.

The final family of structures for domain C0 was obtained using 1360 structural constraints derived from experimental NMR data, including 441 sequential ($i, i + 1$), 85 medium range ($i, i \leq 4$), and 628 long range ($i, i \geq 5$) upper distance limits, 180 backbone torsion angle constraints (90 φ and 90 ψ) produced by the program TALOS (39), and 26 hydrogen bond constraints found in regions with defined secondary structure. Following the final round of CYANA calculation, 81 converged structures were obtained from 100 random starting structures. The converged structures contain no distance or van der Waals violation grater than 0.5 Å and no dihedral angle violations grater than 5° (Table 1).

Differential Scanning Calorimetry—Investigation of thermally induced protein denaturation was performed using a VP-DSC differential scanning calorimeter (MicroCal). Protein samples were in 25 mM MES, pH 7.0, 100 mM NaCl, and 10 mM β-mercaptoethanol and were heated from 10 to 80 °C with constant rate 1 °C/min. Protein concentrations were 80 μM for C0 and C1, 65 μM for S2Δ, 70 μM for RLC, and 65 μM for miniHMM (summarized molecular weights of extended S2Δ and RLC were used for calculation of molar concentration of miniHMM). To obtain information on the reversibility of thermally induced denaturation, samples were heated at the same rate immediately after cooling down after the first denaturation. As some of investigated proteins were unfolding reversibly, we could not use traces obtained from the second denaturation to correct for instrument background. In our experiments, calorimetric traces were therefore corrected by subtracting the scans of the buffer in both cells of the calorimeter. Data were analyzed using Origin 7 software (OriginLab Corp.).

Transfection of MyBP-C Fragments—Cardiac MyBP-C C0 was cloned into an HA-tagged mammalian expression vector as described previously (40). The constructs were transfected into neonatal rat ventricular myocytes using standard procedures, and cells were maintained as described (41). The transfected cells were fixed with 4% paraformaldehyde after 2–3 days in culture, and stained with anti-HA tag antibody (clone 3F10, Roche Applied Science), anti-myosin heavy chain (clone A4.1025, a gift from S. Hughes), and anti α-actinin (Sigma) or Alexa Fluor 633 phalloidin (Molecular Probes) for visualization of F-actin. The specimens were analyzed by confocal microscopy using a Zeiss LSM-510 Meta microscope under 63× magnification and 2–5× zoom.

RESULTS

Structure of Domain C0—The molecular structure of domain C0 was determined using three-dimensional ^{15}N- and ^{13}C-resolved NOESY spectra supplemented by dihedral restraints obtained from chemical shift analysis and hydrogen bond constraints. The NMR data are available from the Biological Magnetic Resonance Bank (accession code 5679), whereas the atomic coordinates were deposited in the Protein Data Bank (2K1M). The good quality of the structure is shown by the high degree of agreement between the 20 structures shown in Fig. 2*A*, which shows 20 of the 81 converged structures as result of the structure calculation carried out with the program CYANA. The average backbone r.m.s.d. is 0.4 Å for the structured portion with the only exception of the N terminus of the domain, which also corresponds to the N terminus of the whole cardiac isoform of MyBP-C, which is completely unstructured (Figs. 2*A* and Fig. 3).

Protein Dynamics Studied by NMR—To confirm the highly disordered nature of the N terminus, the dynamic properties of C0 were studied by ^{15}N relaxation experiments at $T = 298$ K. The relaxation results were analyzed using the Lipari-Szabo approach (32, 33). The rotation correlation time (τ_c) for the domain was determined based on the ratios of the two relaxation times T_1 and T_2, giving a value of 5.81 ± 0.16 ns, in good agreement with the expected value of about 5 ns for a protein of 10 kDa, according to a simple calculation using the Stokes-Einstein equation.

The main result of the Lipari-Szabo analysis is the information about the local rigidity of the molecule, expressed by the order parameter S^2 values determined for each residue (Fig. 3). The plot of S^2 against residue number shows a uniformly rigid structure with S^2 values of 0.8 – 0.9, typical for a well structured protein. In contrast, the N terminus is unstructured with S^2 values dropping to around 0.2 for the first 7– 8 amino acids, in agreement with the r.m.s.d. values (Fig. 3), which are signifi-

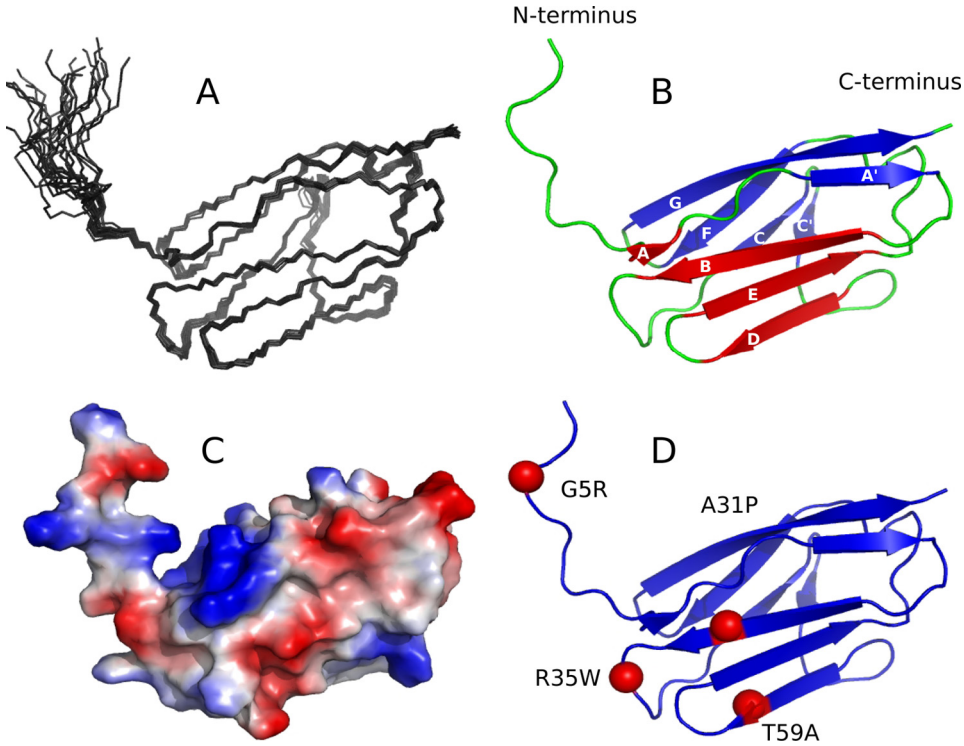

FIGURE 2. **Structure of MyBP-C cardiac-specific domain C0.** *A*, family of 20 structures from the NMR structure calculation. *B*, structure drawings with the two *β*-sheets shown in *red* and *blue*. Strands are labeled according to the standard scheme for the IgI fold. *C*, solvent-accessible surface colored by electrostatic potential. *D*, *α*-carbons of amino acids in C0 mutated in HCM are shown as *red van der Waals spheres*.

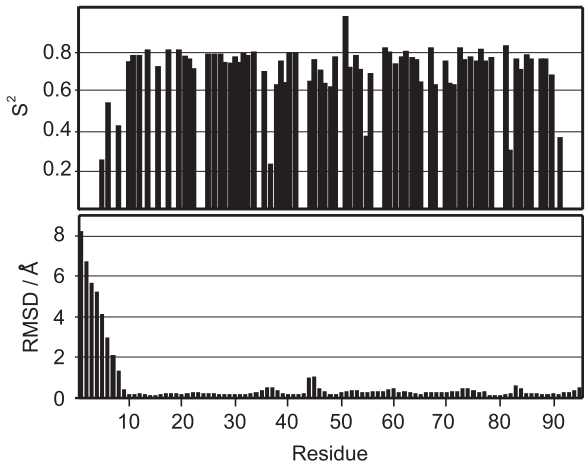

FIGURE 3. **Dynamics of domain C0.** Order parameters S^2 from the Lipari-Szabo analysis of ^{15}N relaxation data are shown in the *top panel*, and average r.m.s.d. values from the top 20 structures in the ensemble are shown in the *bottom panel*. Both are plotted against the sequence.

cantly increased for residues 1–9 when compared with the rest of the protein.

Interaction of C0 with RLC—Based on the results obtained for domains C1 and C2 (14, 15), and in accordance with previous suggestions (16), it was hypothesized that domain C0 could interact, among others, with the RLC. The interaction was investigated *in vitro* using differential scanning calorimetry (DSC), isothermal titration calorimetry (ITC), and NMR spectroscopy, using both RLC bound to its myosin binding site as well as miniHMM and S2Δ as a negative control (Fig. 1).

Differential Scanning Calorimetry—DSC was used to analyze thermally induced denaturation of domain C0, fragments of myosin, and their complexes (as control, domain C1 was also investigated in exactly the same way; supplemental Fig. S1). Thermal denaturation curves of C0 with miniHMM and S2Δ are shown in Fig. 4, *A* and *B*, respectively. In each, the denaturation of C0 alone (*red*), the myosin fragment alone (*green*), and their mixture (*black*) are superimposed. Denaturation of C0 alone is well reproducible with a single well defined peak at a temperature of 57 °C, almost completely reversible (supplemental Fig. S1). Thermal denaturation of miniHMM in Fig. 4*A* shows a sharp peak with a maximum at 50 °C and a broad, less thermostable shoulder with a maximum approximately at 38 °C. The denaturation of S2Δ in Fig. 4*B* has only a single peak around 34 °C, suggesting that the low temperature transition belongs to the coiled-coil portion, whereas the higher temperature transition corresponds to the RLC bound to the myosin binding site. The small increase in melting temperature from S2Δ to miniHMM is likely to be caused by the interaction of the myosin fragment on the RLC. Unfolding of the coiled-coil domain was partially reversible (supplemental Fig. S1) in good agreement with our own data (42, 43).

The experimental denaturation curves of the mixtures of C0 with miniHMM (Fig. 4*A*) and S2Δ (Fig. 4*B*) are markedly different; in the mixture with S2Δ, the denaturation curve is virtually identical to the addition of the two individual curves. The high temperature denaturation peak, corresponding to C0, is slightly shifted by 2 °C to a lower melting temperature, possibly indicating a weak, unspecific interaction. The DSC profile of the denaturation of the mixture of miniHMM and C0 is more complex. At 51.5 °C, a sharp exothermic drop brings the curve to baseline, and then it returns back and forms a shoulder of the main peak. Such an exothermic peak is a very rare effect and normally

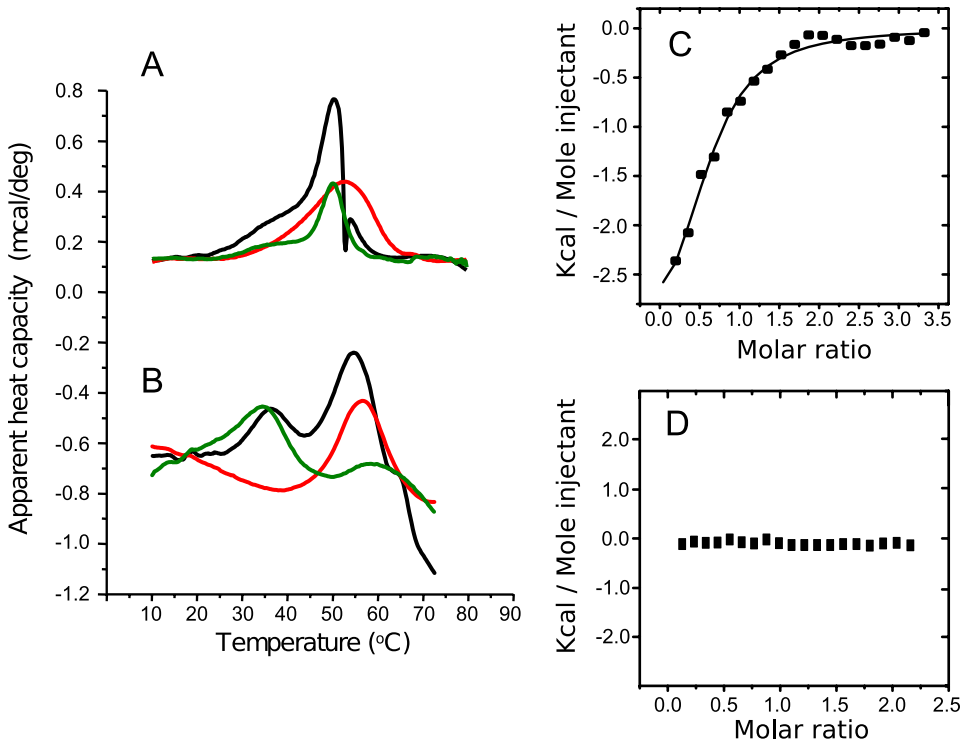

FIGURE 4. **Thermodynamics of the interaction of domain C0 with fragments of myosin.** *A*, interaction of C0 with miniHMM monitored by DSC. *B*, interaction of C0 with S2Δ monitored by DSC. Experimental calorimetric traces of thermally induced denaturation of individual C0 at a concentration of 80 μM (*red*), miniHMM or S2Δ at a concentration of 65 μM (*green line*) and their mixtures (*black line*) are superimposed. *C*, ITC binding curve of C0 with miniHMM. *D*, ITC binding curve of C0 with S2Δ. Experimental data points are shown as *square dots*, and the fitted binding curve is shown as a *continuous line* for *C*. No fitting was possible for *D*.

reflects either fast aggregation (43–45) of proteins in the calorimeter cell or significant changes in protein structure, which occur with release of energy such as chain exchange (45). In our experiments, the appearance of this exothermic peak cannot be explained by aggregation because after the peak, in the temperature region between 60 and 80 °C, the experimental curve follows the baseline and does not have any noise. Furthermore, the sample extracted from the cell after heating did not show any discernible traces of aggregation. This extremely unusual behavior was reproduced in a mixture of C0 with RLC-MyBS (data not shown), suggesting that it is indeed the interaction of C0 with the RLC that causes such an unusual thermodynamic signature. Furthermore, control experiments of miniHMM or RLC-MyBS with C1 did not show any sign of interaction let alone such an unusual exothermic event (data not shown).

Binding of C0 and RLC Studied by ITC—The same mixtures investigated by DSC were also studied by ITC, and the resulting titration curves are shown in Fig. 4*C* for C0 + miniHMM and in Fig. 4*D* for C0 + S2Δ. A very clear binding curve with saturation at an excess of C0 over miniHMM of around 1.5–2.0 confirms an interaction. Fitting the binding curve in Fig. 4*C* yields a dissociation constant of 3.2 ± 1.7 μM and a stoichiometry of C0:miniHMM of 1:0.81 ± 0.16. In contrast, as shown in Fig. 4*D*, no interaction can be detected between domain C0 and S2Δ.

Binding of C0 and RLC Studied by NMR Spectroscopy—Initial interaction studies were performed with purified RLC alone by recording a two-dimensional ^{15}N-^{1}H HSQC spectrum of C0 with increasing concentrations of RLC. Combined ^{1}H/^{15}N chemical shift perturbations were observed but were very noisy, possibly because of limited stability and solubility of the RLC without its binding site (46). To get better data, the interaction was studied instead with miniHMM or RLC-MyBS, which, as expected (47), significantly improved the quality of the chemical shift perturbation data (supplemental Fig. S2). To identify the surface on C0 that takes part in the binding process, the combined ^{1}H/^{15}N chemical shift perturbations due to the protein-protein interaction were plotted against the sequence of C0 (Fig. 5). These plots show very clearly which residues take part in the interaction, mainly charged residues positioned on the surface of the domain. Three regions are most affected by the interaction, a region toward the N terminus (Phe^{12}–Arg^{17}), one around the center of the sequence (Arg^{35}–Val^{38}), and a group of residues toward the C terminus (Ser^{86}–Phe^{90}). Chemical shift perturbations in all these three regions are well above the 2 × σ level for both miniHMM as well as RLC-MyBS, although they are larger for miniHMM. Moreover, in miniHMM, we also see significant perturbations for a fourth region around Ala^{60}, which only has very modest perturbations well below even the 1 × σ level with RLC-MyBS (compare Fig. 6, *top* and *bottom panels*). All perturbed regions are far away from each other in the sequence but find themselves adjoining in the three-dimensional structure, generating a well defined interacting surface positioned toward the N-terminal side of the domain (Fig. 6).

Effects of the HCM-related Mutations in C0 on Binding the RLC—To determine the effect of HCM mutations on C0 structure and function, four mutants were produced of the protein to study their interaction with RLC and to compare their behavior

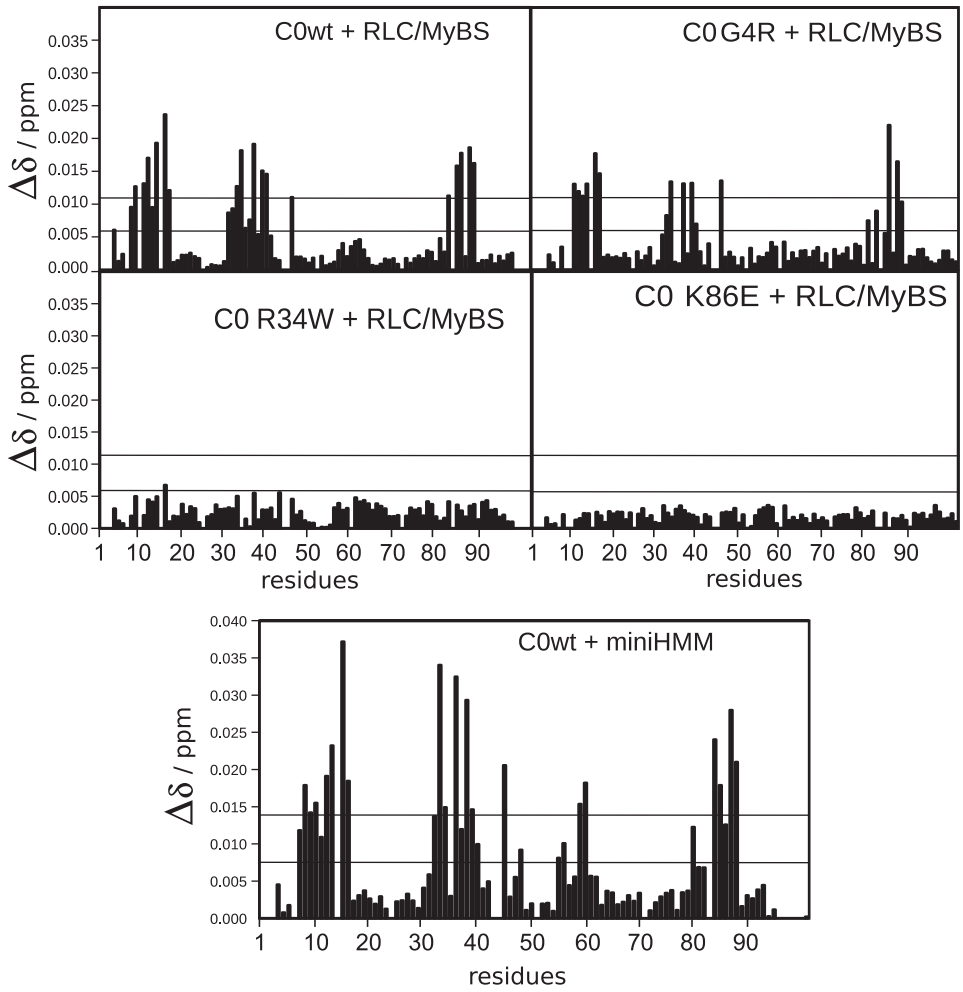

FIGURE 5. **Interaction of domain C0 with the regulatory light chain and other myosin fragments monitored by NMR spectroscopy.** Shown are plots of combined ^{1}H and ^{15}N chemical shift perturbations $\Delta\delta$ of wild type C0 (*C0wt*) and mutated C0 upon the addition of the cardiac regulatory light chain bound to its binding site on myosin and the miniHMM fragment of myosin. The 1 and 2 $\times$ σ levels are indicated by *horizontal lines*.

with wild type C0 used in the previous interaction studies. Three HCM missense mutations have been identified in the human cardiac isoform of domain C0: G5R (48), R35W (see Sarcomeric Gene Mutation Database, MYBPC3_Arg35Trp in the MYBPC3 mutations section, and UniProtKB/Swiss-Prot entry), and T59A (49). For the first two mutations, G5R and R35W, mutants were produced for this investigation, whereas T59A was not chosen as in many other species a threonine residue is substituted by an alanine, and as a consequence, the effect of this mutation is not expected to be extreme, confirmed by clinical studies (49) (supplemental Fig. S3). A third mutant, A31P, was produced as this mutation has been shown to cause cardiac hypertrophy in Maine Coon cats (24) and is associated with a severe phenotype. Finally, the non-HCM mutant K87E was produced to see whether the positive patch around Lys^{87} is involved in the interaction with the RLC. Mutating the lysine residue to glutamic acid should have a significant impact on the interaction and possibly abolish it due to the inversion of charges. All mutants expressed well, apart from A31P, which went into inclusion bodies. The lack of stability of this mutant is confirmed by the clinical observation reported for this mutation (24). The NMR interaction experiments were carried out for G5R, R35W, and K87E using 50 μM ^{15}N-labeled sample of the C0 mutants and 200 μM unlabeled samples of RLC, RLC-MyBS, and miniHMM.

The results are shown alongside the interaction of wild type C0 (wtC0) in Fig. 5. The mutant G5R reduces chemical shift perturbations only mildly, if at all. In contrast, both R35W and K87E have a significant effect on the perturbations, which in both cases are essentially reduced to noise, somewhat more effectively in the case of K87E. This suggests that as expected from the analysis of binding of wild type C0 to RLC-MyBS, both Arg^{35} and Lys^{87} are important for binding, whereas the lack of an effect of G5R despite its location right next to the binding site is somewhat unexpected.

Immunofluorescence Localization of C0 in Primary Cardiomyocytes—We wanted to determine whether the biochemically and biophysically determined interaction between RLC and C0 was sufficiently strong to be detectable also in C0-expressing neonatal rat cardiomyocytes. When we transfected neonatal rat cardiomyocytes with HA-tagged C0, we observed sarcomeric localization in doublet stripes (Fig. 7) that completely co-localized in the A-band with the A4.1025 monoclonal antibody against the motor domain of sarcomeric myosin (50). In contrast, the I-band region around the Z-disk (stained against α-ac-

tinin) and the bare zone at the center of the A-band (spared also in the A4.1025 stain) did not show C0 localization. These results suggest that C0 is targeted to the cross-bridge region of the myosin filament but shows no appreciable enrichment with myosin rods (bare zone) or actin filaments (I-band). In the cellular context, the interactions of C0 with sarcomeric proteins are therefore dominated by myosin interactions in the motor domain region.

DISCUSSION

Structure of Domain C0—As expected, the structure of domain C0 conforms to the IgI fold (51) typical of the majority of MyBP-C IgI domains, formed by a β-sandwich composed of two β-sheets, ABED and C′CFGA′, respectively (Fig. 2*B*) including the once controversial C′ strand (52). The hydrophobic core of the protein is well defined by the aromatic residues Trp^{42}, which is highly conserved through species and is central to the domain stability, and Tyr^{79}, which is involved in the tyrosine corner (53) (Fig. 6*A*), another characteristic feature of these domains. Because of the presence of the β-bulge (54), strand A is very short and poorly defined so that only one hydrogen bond can be formed between Lys^{14} and Glu^{32} in strand B. Although the sequence conservation of strand A is the lowest within the IgI fold, the high degree of conservation of a phenylalanine at the start in most IgI domains of MyBP-C is noteworthy. The β-bulge is a recurring feature of IgI domains, and it is present in all other MyBP-C IgI domains of known structure, being grossly enlarged in domain C5 (6). Apart from the short strand A, the N terminus of C0, which comprises resides 1–12, is highly unstructured, the only poorly defined part of the domain (Fig. 2*A*). The apparent structural disorder is caused by genuine flexibility and dynamics, as shown in Fig. 3. This could be an important aspect of C0 function as the N terminus could be able to reach out to interact with other muscle proteins. This hypothesis is supported by the presence of three prolines, amino acids often involved in protein-protein interactions. One of these is only found in mammals, suggesting a specific adaptation.

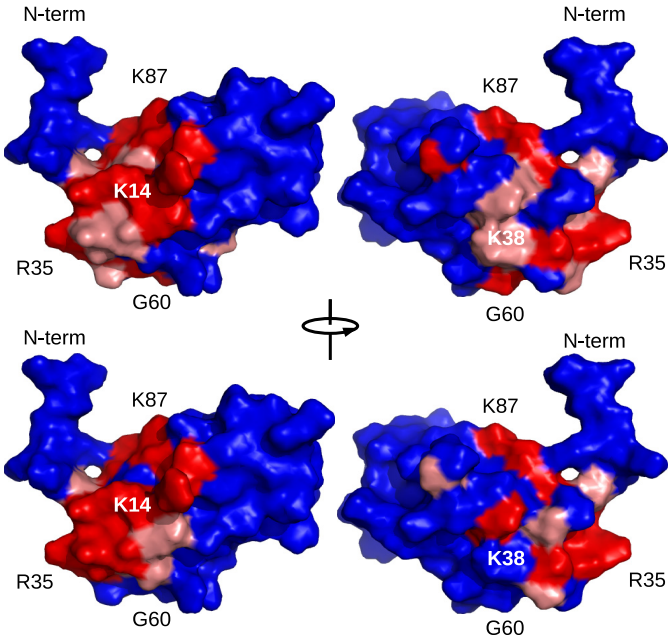

FIGURE 6. **Mapping of chemical shift perturbations on the surface of domain C0.** The solvent-exposed surface is shown in two views rotated by 180° about the vertical axis as indicated. Chemical shift perturbations for interaction with miniHMM (*top*) and RLC-MyBS (*bottom*) are shown by *red* for perturbations $>2\sigma$ and in *salmon* for perturbations between 1 and 2σ. Selected amino acids are labeled to aid orientation. Amino acids with perturbations $<1\sigma$ are shown in *blue*.

Interaction between C0 of Cardiac MyBP-C and RLC—Our combined data from DSC, ITC, and NMR clearly show that domain C0 binds to the RLC when bound to only its myosin binding site or as part of the miniHMM complex. No interaction to the S2 portion of myosin could be detected, in contrast to domains C1 and C2 (10, 14, 15). Myosin binding of C0 was subsequently confirmed *in vivo* by co-localization with the myosin motor domain in neonatal rat cardiomyocytes (Fig. 7), in contrast to the previously suggested interaction with the thin filament (55, 56). Such an interaction should produce a very different staining profile. The binding itself, as monitored by DSC, is most unusual as the resulting complex melts with a very surprising exothermic peak (Fig. 4*A*), which is only very rarely seen. It is found for the interaction of C0 both with RLC-MyBS as well as with miniHMM, suggesting that it is not a feature of the S1-S2 junction. Instead, this peculiar thermodynamic feature must be a property of the C0-RLC interface. The observation of deviations from a standard titration curve in the ITC experiments lends support to this unusual thermodynamic behavior. Given the conformational flexibility built into proteins of the EF-hand family, it is interesting to speculate that this feature could signal a conformational change in the RLC, which might be an important functional feature, related to the observations of the effects of N-terminal MyBP-C fragments (12, 13). NMR mapping of the binding site for RLC on C0 clearly identifies a very large region toward to N terminus of the domain that forms a continuous, mainly positively charged sur-

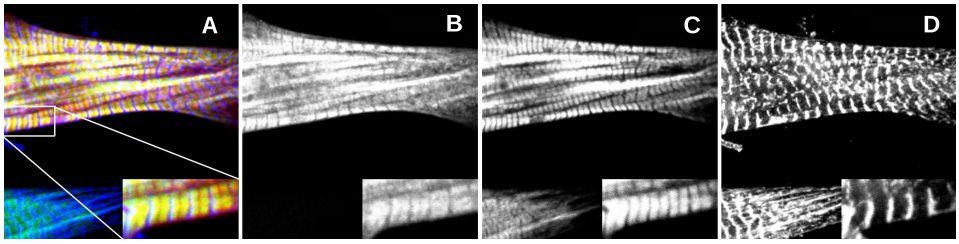

FIGURE 7. **Neonatal rat cardiac myocytes after transfection with HA-tagged C0 stained for the HA tag (*red* in overlay in *A* and *B*) or for MHC (*green* in overlay in *A* and *C*) and α-actinin (*blue* in overlay in *A* and *D*).** The center of the A-band (comprising the H- and M-band) is marked by *arrowheads*. *Inset panels* demonstrate clear co-localization of the transfected MyBP-C C0 fragment with myosin heads stained by the A4.1025 antibody (*yellow* in overlay *in panel A*), sparing the bare zone at the myosin filament center (*arrowheads*) as well as the I-Z-I region (*blue* α-actinin staining).

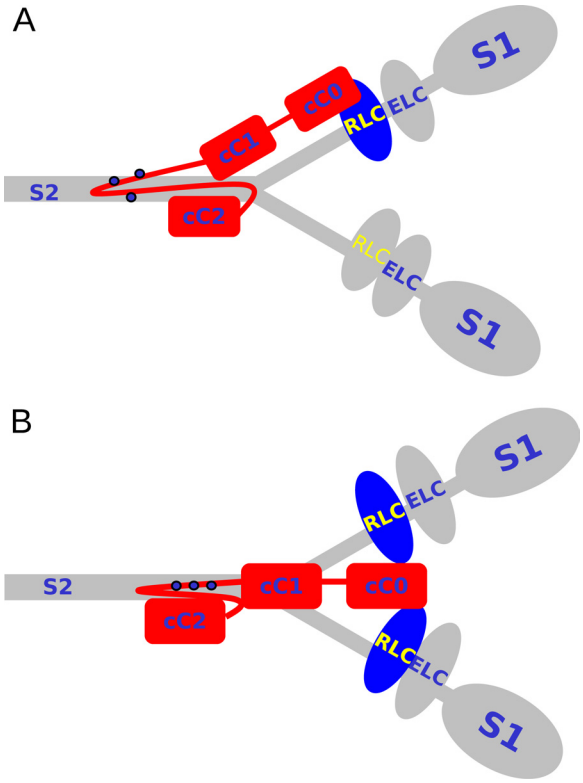

FIGURE 8. **Model for the arrangement of the N terminus of MyBP-C around the myosin S1-S2 junction and the light chains.** MyBP-C domains C1 and C2 bind to S2 very close to the junction, whereas C0 binds to the RLC. In *A*, binding of C0 to RLC could happen as shown here, where the 2:1 stoichiometry leads to an asymmetry of the two S1 heads, which could be the main purpose of the interaction. In *B*, the NMR and ITC data are interpreted as a pseudosymmetric interaction of C0 with both RLCs simultaneous, whereby C0 is wedged in between the RLCs.

face (Fig. 6), in good agreement with the small magnitude of the chemical shift perturbations.

No chemical shift perturbations are seen for the flexible N-terminal ~10 amino acids despite being in immediate spatial proximity to the binding site (Figs. 5 and 6). This suggests that this portion of the protein is not involved in binding to RLC but might interact with other muscle proteins. Potential candidates could be domain C1, which has a potential second binding surface (14) oriented in a suitable manner, or the nearby ELC. According to our immunofluorescence data, it appears less likely that this portion of domain C0 could interact with actin (55, 57).

To investigate the C0-RLC interaction further, point mutations were designed based on their connection to HCM (G5R, A31P, and R35W) or the NMR binding surface (K87E). Of these, only A31P was not expressed as a soluble protein, possibly because of a loss of stability of the domain similar to other familial hypertrophic cardiomyopathy-related mutations in different MyBP-C domains (6, 14). The G5R mutation had very little effect, whereas chemical shift perturbations for R35W and K87E are extremely weak, and no regions of residues affected by the interaction are clearly identifiable. The results of these three mutations agree very well with their location on the protein surface.

The functional implications of our findings are summarized in Fig. 8, where two modes of C0-RLC interactions are shown. Our *in vitro* stoichiometry combined with the large surface of C0 perturbed in the NMR mapping experiments suggest that one C0 could bind to both RLCs simultaneously. As a result, it could be positioned between the RLCs as shown in Fig. 8*B*. In such a position, C0 would be very well positioned to influence the relative orientation of the S1 heads, about which very little is known (58). Wedging C0 between the RLCs could either push the S1 heads apart or pull them together. C0 could be removed to restore flexibility *e.g.* by RLC phosphorylation, which is known to modulate the general activity of myosin in a manner not dissimilar to MyBP-C (23). The possibility that C0 interplays with RLC phosphorylation, either by modulating the interaction between RLC and C0 or by modulating the phosphorylation of RLC, will be interesting to investigate.

Acknowledgment—We thank Fred Muskett for help with NMR spectrometers.

REFERENCES

1. Oakley, C. E., Hambly, B. D., Curmi, P. M., and Brown, L. J. (2004) *Cell Res.* **14,** 95–110
2. Winegrad, S. (2000) *Circ. Res.* **86,** 6–7
3. Winegrad, S. (2003) *Adv. Exp. Med. Biol.* **538,** 31–41
4. Bennett, P. M., Fürst, D. O., and Gautel, M. (1999) *Rev. Physiol. Biochem. Pharmacol.* **138,** 203–234
5. Gautel, M., Zuffardi, O., Freiburg, A., and Labeit, S. (1995) *EMBO J.* **14,** 1952–1960
6. Idowu, S. M., Gautel, M., Perkins, S. J., and Pfuhl, M. (2003) *J. Mol. Biol.* **329,** 745–761
7. Weisberg, A., and Winegrad, S. (1996) *Proc. Natl. Acad. Sci. U.S.A.* **93,** 8999–9003
8. McClellan, G., Kulikovskaya, I., and Winegrad, S. (2001) *Biophys. J.* **81,** 1083–1092
9. Levine, R., Weisberg, A., Kulikovskaya, I., McClellan, G., and Winegrad, S. (2001) *Biophys. J.* **81,** 1070–1082
10. Gruen, M., Prinz, H., and Gautel, M. (1999) *FEBS Lett.* **453,** 254–259
11. Kunst, G., Kress, K. R., Gruen, M., Uttenweiler, D., Gautel, M., and Fink, R. H. A. (2000) *Circ. Res.* **86,** 51–58
12. Herron, T. J., Rostkova, E., Kunst, G., Chaturvedi, R., Gautel, M., and Kentish, J. C. (2006) *Circ. Res.* **98,** 1290–1298
13. Harris, S. P., Rostkova, E., Gautel, M., and Moss, R. L. (2004) *Circ. Res.* **95,** 930–936
14. Ababou, A., Rostkova, E., Mistry, S., Le Masurier, C., Gautel, M., and Pfuhl, M. (2008) *J. Mol. Biol.* **384,** 615–630
15. Ababou, A., Gautel, M., and Pfuhl, M. (2007) *J. Biol. Chem.* **282,** 9204–9215
16. Margossian, S. S. (1985) *J. Biol. Chem.* **260,** 13747–13754
17. Rayment, I., Rypniewski, W. R., Schmidt-Bäse, K., Smith, R., Tomchick, D. R., Benning, M. M., Winkelmann, D. A., Wesenberg, G., and Holden, H. M. (1993) *Science* **261,** 50–58
18. Xie, X., Harrison, D. H., Schlichting, I., Sweet, R. M., Kalabokis, V. N., Szent-Györgyi, A. G., and Cohen, C. (1994) *Nature* **368,** 306–312
19. Margossian, S. S., and Slayter, H. S. (1987) *J. Muscle Res. Cell. Motil.* **8,** 437–447
20. Takashima, S. (2009) *Circ. J.* **73,** 208–213
21. Scruggs, S. B., Hinken, A. C., Thawornkaiwong, A., Robbins, J., Walker, L. A., de Tombe, P. P., Geenen, D. L., Buttrick, P. M., and Solaro, R. J. (2009) *J. Biol. Chem.* **284,** 5097–5106
22. Davis, J. S., Hassanzadeh, S., Winitsky, S., Lin, H., Satorius, C., Vemuri, R., Aletras, A. H., Wen, H., and Epstein, N. D. (2001) *Cell* **107,** 631–641
23. Colson, B. A., Locher, M. R., Bekyarova, T., Patel, J. R., Fitzsimons, D. P., Irving, T. C., and Moss, R. L. (2010) *J. Physiol.* **588,** 981–993
24. Meurs, K. M., Sanchez, X., David, R. M., Bowles, N. E., Towbin, J. A.,

Reiser, P. J., Kittleson, J. A., Munro, M. J., Dryburgh, K., Macdonald, K. A., and Kittleson, M. D. (2005) *Hum. Mol. Genet.* **14,** 3587–3593
25. Gruen, M., and Gautel, M. (1999) *J. Mol. Biol.* **286,** 933–949
26. Clore, G. M., and Gronenborn, A. M. (1991) *Annu. Rev. Biophys. Biophys. Chem.* **20,** 29–63
27. Grzesiek, S., and Bax, A. (1992) *J. Am. Chem. Soc.* **114,** 6291–6293
28. Wang, A. C., Lodi, P. J., Qin, J., Vuister, G. W., Gronenborn, A. M., and Clore, G. M. (1994) *J. Magn. Reson.* **105,** 196–198
29. Bax, A., Clore, M., Driscoll, P. C., Gronenborn, A. M., Ikura, M., and Kay, L. E. (1990) *J. Magn. Reson.* **87,** 620
30. Majumdar, A., and Zuiderweg, E. P. (1993) *J. Magn. Reson.* **102,** 242
31. Barbato, G., Ikura, M., Kay, L. E., Pastor, R. W., and Bax, A. (1992) *Biochemistry* **31,** 5269–5278
32. Lipari, G., and Szabo, A. (1982) *J. Am. Chem. Soc.* **104,** 4546–4559
33. Lipari, G., and Szabo, A. (1982) *J. Am. Chem. Soc.* **104,** 4559–4570
34. Clore, G. M., Szabo, A., Bax, A., Kay, L. E., Driscoll, P. C., and Gronenborn, A. M. (1990) *J. Am. Chem. Soc.* **112,** 4989–4991
35. Gronenborn, A. M., Bax, A., Wingfield, P. T., and Clore, G. M. (1989) *FEBS Lett.* **243,** 93–98
36. Mulder, F. A., Schipper, D., Bott, R., and Boelens, R. (1999) *J. Mol. Biol.* **292,** 111–123
37. Herrmann, T., Güntert, P., and Wüthrich, K. (2002) *J. Biomol. NMR* **24,** 171–189
38. Güntert, P., Mumenthaler, C., and Wüthrich, K. (1997) *J. Mol. Biol.* **273,** 283–298
39. Cornilescu, G., Delaglio, F., and Bax, A. (1999) *J. Biomol. NMR* **13,** 289–302
40. Lange, S., Himmel, M., Auerbach, D., Agarkova, I., Hayess, K., Fürst, D. O., Perriard, J. C., and Ehler, E. (2005) *J. Mol. Biol.* **345,** 289–298
41. Auerbach, D., Bantle, S., Keller, S., Hinderling, V., Leu, M., Ehler, E., and Perriard, J. C. (1999) *Mol. Biol. Cell* **10,** 1297–1308
42. Holtzer, M. E., and Holtzer, A. (1990) *Biopolymers* **30,** 985–993
43. Levitsky, D. I., Rostkova, E. V., Orlov, V. N., Nikolaeva, O. P., Moiseeva, L. N., Teplova, M. V., and Gusev, N. B. (2000) *Eur. J. Biochem.* **267,** 1869–1877
44. Merabet, E. K., Walker, M. C., Yuen, H. K., and Sikorski, J. A. (1993) *Biochim. Biophys. Acta* **1161,** 272–278
45. Orlov, V. N., Rostkova, E. V., Nikolaeva, O. P., Drachev, V. A., Gusev, N. B., and Levitsky, D. I. (1998) *FEBS Lett.* **433,** 241–244
46. Ratti, J. (2009) *Investigation of cardiac myosin binding protein C (cMyBPC) domains and their interactions*. Ph.D. thesis, University of Leicester
47. Bagshaw, C. R. (1977) *Biochemistry* **16,** 59–67
48. Van Driest, S. L., Vasile, V. C., Ommen, S. R., Will, M. L., Tajik, A. J., Gersh, B. J., and Ackerman, M. J. (2004) *J. Am. Coll. Cardiol.* **44,** 1903–1910
49. Niimura, H., Patton, K. K., McKenna, W. J., Soults, J., Maron, B. J., Seidman, J. G., and Seidman, C. E. (2002) *Circulation* **105,** 446–451
50. Dan-Goor, M., Silberstein, L., Kessel, M., and Muhlrad, A. (1990) *J. Muscle Res. Cell. Motil.* **11,** 216–226
51. Harpaz, Y., and Chothia, C. (1994) *J. Mol. Biol.* **238,** 528–539
52. Mayans, O., Wuerges, J., Canela, S., Gautel, M., and Wilmanns, M. (2001) *Structure* **9,** 331–340
53. Hemmingsen, J. M., Gernert, K. M., Richardson, J. S., and Richardson, D. C. (1994) *Protein Sci.* **3,** 1927–1937
54. Richardson, J. S., Getzoff, E. D., and Richardson, D. C. (1978) *Proc. Natl. Acad. Sci. U.S.A.* **75,** 2574–2578
55. Whitten, A. E., Jeffries, C. M., Harris, S. P., and Trewhella, J. (2008) *Proc. Natl. Acad. Sci. U.S.A.* **105,** 18360–18365
56. Shaffer, J. F., Kensler, R. W., and Harris, S. P. (2009) *J. Biol. Chem.* **284,** 12318–12327
57. Jeffries, C. M., Whitten, A. E., Harris, S. P., and Trewhella, J. (2008) *J. Mol. Biol.* **377,** 1186–1199
58. Offer, G., and Knight, P. J. (1996) *J. Mol. Biol.* **256,** 407–416